REVIEW

This section of Journal of Materials Research is reserved for papers that are reviews of literature in a given area.

Orbital-free density functional theory for materials research

William C. Witt, Beatriz G. del Rio, and Johannes M. Dieterich
Department of Mechanical and Aerospace Engineering, Princeton University, Princeton, New Jersey 08544-5263, USA

Emily A. Carter[a)]
School of Engineering and Applied Science, Princeton University, Princeton, New Jersey 08544-5263, USA

Orbital-free density functional theory (OFDFT) is both grounded in quantum physics and suitable for direct simulation of thousands of atoms. This article describes the application of OFDFT for materials research over roughly the past two decades, highlighting computational studies that would have been impractical (or impossible) to perform with other techniques. In particular, we review the growing body of simulations of solids and liquids that have been conducted with planewave-pseudopotential (or related) techniques. We also provide an updated account of the fundamentals of OFDFT, emphasizing aspects—such as nonlocal density functionals for computing the kinetic energy of noninteracting electrons—that enabled much of the application work. The article concludes with a discussion of the OFDFT frontier, which contains brief descriptions of other topics at the forefront of OFDFT research.

I. INTRODUCTION

Some of the most challenging problems in materials science—and many ordinary ones too—require a theory and computing strategy that is grounded in quantum physics and suitable for simultaneous study of thousands of atoms. Crystalline alloys with motifs of tens or hundreds of atoms are one straightforward example; for these solids, supercells of several repeated unit cells can quickly cross the thousand-atom threshold. Dislocations in metals are another example; these defects are characterized both by local disruptions in periodicity and by a long-ranged elastic strain field that can interact with other dislocations or grain boundaries. Finally, it is well known that ab initio molecular dynamics (MD) simulations are useful for probing the structure of liquids but only if a sufficient number of atoms are included to prevent spurious correlations.

Orbital-free (OF)[1–4] density functional theory (DFT),[5–7] rooted in quantum mechanics, is an especially promising tool for the materials community. Its principal advantages over standard Kohn–Sham (KS)[8] DFT are speed and computational scaling: as the number of atoms in a simulation increases, the computational effort required for OFDFT can be made to scale linearly [or quasi-linearly, $O(N \log N)$] with a small prefactor. The chief aim of this article is to review the application of OFDFT for materials research over roughly the past two decades, highlighting examples where OFDFT was, and remains, perhaps the only tool available. Before doing so, we give an updated overview of the fundamentals, emphasizing the aspects of the theory that enabled most of the application work. We conclude with a short discussion of the OFDFT frontier, along with some additional remarks.

Before proceeding, we note a few important avenues of inquiry that fall within the broader OFDFT field but are not discussed in detail in this article. The first is the study of warm dense matter,[9] in which OF methods are finding increasing use. We do discuss a very small number of examples in this category, but do not give a detailed account of the field, nor of functionals with explicit temperature dependence. Second, we do not discuss subsystem DFT nor the OF functionals designed specifically with this purpose in mind. Instead, we refer readers to several review articles on this topic[10,11] and to the second part of a recent volume on OFDFT.[3] Finally, our discussion of OF functionals for the noninteracting kinetic energy is limited to the subset of nonlocal functionals most directly connected to the application work that is our primary focus. However, we do reference recent advances in the design of single-point functionals in Sec. IV on the OFDFT frontier.

II. THEORY AND IMPLEMENTATION

The fundamentals of OFDFT[1–4] and DFT more generally[5–8] are described in a great number of references.

© Materials Research Society 2017

For completeness, we review the most salient points here. In principle, for a system of electrons subject to an external potential $v(\mathbf{r})$, one may find its ground-state energy by varying the electron distribution $n(\mathbf{r})$ to minimize an energy functional

$$E[n] = T_{\rm s}[n] + E_{\rm H}[n] + E_{\rm xc}[n] + \int d\mathbf{r}\, v(\mathbf{r})n(\mathbf{r}) \quad , \quad (1)$$

all while requiring $n(\mathbf{r}) \geq 0$ and maintaining the proper number of electrons, N, with the normalization constraint $\int d\mathbf{r}\, n(\mathbf{r}) = N$. The first three terms on the right-hand side of Eq. (1) are the noninteracting electron kinetic energy $T_{\rm s}[n]$, the electrostatic repulsion between electrons $E_{\rm H}[n]$, and the energy attributed to the quantum-mechanical exchange and correlation $E_{\rm xc}[n]$ (which includes the difference between the interacting kinetic energy and $T_{\rm s}[n]$). These terms together comprise the universal functional first identified in the landmark paper by Hohenberg and Kohn,[7] whose work undergirds the vast enterprise of DFT research. The final term in Eq. (1) describes the interaction between the electrons and the external potential $v(\mathbf{r})$.

For a system composed of atoms, $v(\mathbf{r})$ is generated as a superposition of individual atomic potentials. All-electron calculations employ Coulombic nuclear potentials, while valence-electron-only calculations utilize pseudopotentials that model the combined effect of core electrons and the nuclear charge (the latter combination is referred to as an ion). The total system energy, then, is obtained by adding the appropriate ion–ion interaction energy to Eq. (1). In addition, one can use DFT to determine the forces exerted on individual atoms and the state of stress in a crystal. These properties are computed, in short, by probing the change in system energy induced by infinitesimal displacements of atoms (for forces) or infinitesimal adjustments to the crystal lattice (for stresses).

The usual approach to DFT—and also the particular decomposition of terms given in Eq. (1)—is attributable to Kohn and Sham,[8] who devised an implicit strategy for computing the exact value of $T_{\rm s}[n]$. To accomplish this task, KSDFT relies on self-consistently determined one-electron wave functions for a reference system of non-interacting electrons with an electron density that is identical to that of the fully interacting system. Therefore, because the classical electrostatic repulsion term is known explicitly, $E_{\rm H}[n] = 1/2 \int d\mathbf{r} \int d\mathbf{r}' n(\mathbf{r})n(\mathbf{r}')/|\mathbf{r} - \mathbf{r}'|$, only the exchange-correlation energy $E_{\rm xc}[n]$ must be approximated, and this term is expected to be relatively smaller in magnitude than the others. A downside of the one-particle wave function approach is that wave function operations give rise to cubic computational scaling: a doubling of the number of electrons in a simulation tends to increase the computational effort by a factor of eight. This feature of standard KSDFT renders it unappealing, and frequently prohibitive, for simulations involving many hundreds or thousands of atoms. Finally, while KSDFT is not the focus of this article, it is appropriate at this stage to mention the burgeoning field of (quasi-)linear-scaling KSDFT. Although a certain level of maturity has been reached for insulating systems, this topic remains an active area of research.[12–14]

In OFDFT, $T_{\rm s}[n]$ is computed directly from the electron density rather than indirectly from single-particle wave functions. This original formulation bypasses wave functions entirely, and the simplification in formalism enables DFT simulations with (quasi-)linear computational scaling and a small prefactor. However, an approximation is required because, as with the case of $E_{\rm xc}[n]$, no exact, easily evaluated form for $T_{\rm s}[n]$ is known. (Importantly, OFDFT formulated in this way makes use of the same exchange-correlation functionals that have propelled KSDFT to prominence.) In the following subsection, we introduce a series of approximations for $T_{\rm s}[n]$ that have been applied in materials science research. Subsequently, because many OFDFT studies utilize pseudopotentials to reduce computational expense, we describe the theory of local pseudopotentials (LPSs). Finally, in the concluding subsection, we discuss computational strategies and algorithmic best practices that enable efficient OFDFT calculations.

A. Kinetic energy density functionals

The discussion on kinetic energy density functionals (KEDFs) is divided into three parts. First, we present three relatively simple approximations for $T_{\rm s}[n]$, each of which yields the exact result for a certain special case, and then use these examples to develop a preliminary understanding of the philosophy that underlies the nonlocal functionals used in most of the application work described later. Second, we describe two paradigms that began to emerge during the period between 1985 and 2000. Most of the OFDFT studies chronicled in the latter half of this article rely on approximations for $T_{\rm s}[n]$ that fall within these two categories. Finally, we discuss a series of more recent attempts to improve on the performance of earlier nonlocal functionals.

This treatment is not intended to be a comprehensive review of the full canon of KEDFs. Instead, we emphasize the subset of predominantly nonlocal functionals that provide near-KSDFT accuracy for a limited portion of the periodic table; these functionals enabled most of the research on solid and liquid materials described subsequently. Interested readers will find more information in several review articles that cover KEDFs more broadly[1,6,15,16] and, in addition, we provide an extremely brief discussion on recent advances in single-point KEDF development later in Sec. IV.

1. Three simple approximations for $T_s[n]$

a. Single-orbital systems and the von Weizsäcker functional

For a single, isolated electron in a static external potential, one can infer a ground-state wave function by computing the square root of the ground-state electron density, and thereby obtain from elementary quantum mechanics the exact $T_s[n]$ for this simple system. The result was first published by von Weizsäcker[17] (vW) in 1935 and may be written as

$$T_{vW}[n] = -\frac{1}{2} \int dr n^{1/2}(\mathbf{r}) \nabla^2 n^{1/2}(\mathbf{r})$$
$$= \frac{1}{2} \int dr \nabla n^{1/2}(\mathbf{r}) \cdot \nabla n^{1/2}(\mathbf{r}) \quad . \quad (2)$$

The vW functional also provides the exact non-interacting kinetic energy for other single-orbital systems in their ground state, such as two spin-unpolarized electrons or any number of bosons. When applied to systems of many fermions, $T_{vW}[n]$ returns a rigorous lower bound to the full $T_s[n]$ and therefore the following expression is general: $T_s[n] \geq T_{vW}[n]$. The two forms of $T_{vW}[n]$ given in Eq. (2) are related by the divergence theorem and they are equivalent for isolated systems and for systems described with periodic boundary conditions.

b. The free-electron gas and the Thomas–Fermi functional

The free-electron gas is so-named because its members traverse freely across a perfectly flat potential landscape, encumbered only by the Pauli Exclusion Principle. It is generally regarded as the simplest many-fermion system, and its electron density and other properties are constant throughout space; that is, $n(\mathbf{r}) \to n_0$. The relationship between the kinetic energy (per unit volume) and the electron density is given by $t_0 = c_0 n_0^{5/3}$, where $c_0 = (3/10)(3\pi^2)^{2/3}$ is the appropriate constant for spin-unpolarized electrons.

For more general systems with slowly varying electron densities, a reasonable approximation to the kinetic energy is obtained if one applies the free-electron-gas expression locally, and integrates. This functional,

$$T_{TF}[n] = c_0 \int dr\, n^{5/3}(\mathbf{r}) \quad , \quad (3)$$

was proposed independently by Thomas[18] and Fermi[19] (TF) in 1927 and it represents the earliest approximation for $T_s[n]$ from a historical perspective. Because $T_{TF}[n]$ encodes the Pauli Exclusion Principle, it may also serve as a crude approximation to the excess kinetic energy not accounted for by $T_{vW}[n]$. The combination $T_{vW}[n] + T_{TF}[n]$ remains exact for a uniform electron gas but introduces error for any single-orbital system.

c. Weakly perturbed free-electron gas

When $n(\mathbf{r})$ deviates only modestly from uniformity—more precisely, when $n(\mathbf{r}) = n_0 + \Delta(\mathbf{r})$ with $|\Delta(\mathbf{r})| \ll n_0$ and $\int dr \Delta(\mathbf{r}) = 0$—the kinetic energy $T_s[n]$ may be obtained with high accuracy from the second-order perturbation expansion for a free-electron gas

$$T_2[n] = T_{TF}[n_0] + \frac{1}{2} \int dr \int dr' \Delta(\mathbf{r}) \frac{\delta^2 T_s}{\delta n(\mathbf{r})\delta n(\mathbf{r}')}\bigg|_{n_0} \Delta(\mathbf{r}') \quad . \quad (4)$$

The second functional derivative in Eq. (4) is known exactly and is closely associated with the Lindhard[20] density–density response function, $\chi_0(\mathbf{k})$. The exact relationship is given by

$$F\left[\frac{\delta^2 T_s}{\delta n(\mathbf{r})\delta n(\mathbf{r}')}\bigg|_{n_0}\right] = -\frac{1}{\chi_0(\mathbf{k})} \quad , \quad (5)$$

where $F[\cdot]$ indicates a Fourier transform. For spin-unpolarized electrons, $\chi_0(\mathbf{k})$ has the analytical form $\chi_0(\mathbf{k}) = -(k_0/\pi^2)f(k/2k_0)$, where $k = |\mathbf{k}|$, $k_0 = (3\pi^2 n_0)^{1/3}$, and

$$f(x) = \frac{1}{2} + \frac{1-x^2}{4x} \ln\left|\frac{1+x}{1-x}\right| \quad . \quad (6)$$

d. Combining the three approximations

Each of these elementary approximations for $T_s[n]$ is exact in a certain limit and becomes accurate as an electron density approaches that limit. Consider now the composite functional that one would obtain by starting with $T_2[n]$—which is correct to second order for a perturbed free-electron gas—and then adding estimated contributions for the third and higher order terms using corrections derived from, say, $T_{vW}[n] + T_{TF}[n]$. Such a functional would remain accurate for a weakly perturbed electron gas but would potentially be more accurate than $T_2[n]$ by itself for other systems. In fact, this functional, considered by Perrot,[21] is emblematic of a category of functionals initiated by Wang and Teter,[22] which is one of the two categories discussed in the following subsection.

2. Nonlocal functionals based on the Lindhard response function

Most of the materials science studies described in this review were enabled by two classes of approximations for $T_s[n]$ that both incorporate the Lindhard response

function, $\chi_0(\mathbf{k})$. The connection between $T_s[n]$ and $\chi_0(\mathbf{r})$—namely, Eq. (5)—was apparent even during the earliest stages of DFT research.[7] The functionals described in this section all satisfy Eq. (5) by construction and, as a result, are able to predict expected quantum-mechanical features such as shell structure in atoms and Friedel oscillations in metals. Moreover, a sizable subset of these functionals may be evaluated with (quasi-)linear-scaling computational effort.

a. The Chacón–Alvarellos–Tarazona functional and generalizations

The Chacón–Alvarellos–Tarazona (CAT) functional[23] was introduced in 1985, and its key ingredient has the form

$$T^{\mathrm{nl}}_{\mathrm{CAT}}[n] = c_0 \int \mathrm{d}\mathbf{r}\, n(\mathbf{r})\bar{n}^{2/3}(\mathbf{r}) \quad , \qquad (7)$$

in which $\bar{n}(\mathbf{r})$ refers to a yet unspecified average density, where the averaging procedure probes the fluctuations in $n(\mathbf{r})$ near the point $\mathbf{r}$. The expression in Eq. (7) clearly resembles the TF functional—and it is identical to $T_{\mathrm{TF}}[n]$ for the limiting case of a free-electron gas—but it also incorporates the extra, nonlocal information that is encoded in $\bar{n}(\mathbf{r})$. In the original CAT functional, $\bar{n}(\mathbf{r})$ is obtained from a spherical average $\bar{n}(\mathbf{r}) = \int \mathrm{d}\mathbf{r}' w(k_0(\mathbf{r}), |\mathbf{r} - \mathbf{r}'|)n(\mathbf{r}')$, where $k_0(\mathbf{r})$ is the local Fermi wave vector, $k_0(\mathbf{r}) = (3\pi^2 n(\mathbf{r}))^{1/3}$. The weight function $w(k_0(\mathbf{r}), |\mathbf{r} - \mathbf{r}'|)$ is chosen such that the overall functional satisfies Eq. (5), thereby ensuring that it returns the correct result for a weakly perturbed electron gas.

Over time, a variety of modifications to the CAT functional have appeared;[16,24–29] however, the original spirit is preserved in each case cited. One prominent generalization involves the introduction of a symmetrized, two-point Fermi wave vector, $k_0(\mathbf{r}) \rightarrow k_0^\gamma(\mathbf{r}, \mathbf{r}')$, which transforms the spherical average used initially to obtain $\bar{n}(\mathbf{r})$ into a nonspherical average to better incorporate nonlocal effects.[25] Another more recent modification attempts to improve the accuracy of CAT-like functionals for localized systems.[27] Finally, while the most natural implementations of the CAT functional incurs quadratic computational scaling, several simplifications that are appropriate for extended systems may be evaluated with (quasi-)linear scaling.[16,27–29]

b. The Wang–Teter, Perrot, Smargiassi–Madden, and Wang–Govind–Carter functionals

A second category of nonlocal approximations for $T_s[n]$ is composed of contributions from a variety of authors, each published between 1992 and 1999. The earliest was put forth by Wang and Teter[22] and may be written as

$$T_{\mathrm{WT}}[n] = T_{\mathrm{vW}}[n] + T_{\mathrm{TF}}[n]$$
$$+ \int \mathrm{d}\mathbf{r} \int \mathrm{d}\mathbf{r}'\, n^{5/6}(\mathbf{r})w(k_0, |\mathbf{r} - \mathbf{r}'|)n^{5/6}(\mathbf{r}') \quad .$$
$$(8)$$

In Eq. (8), k_0 refers to the Fermi-wave vector associated with a fixed reference density n_0, and the integral kernel $w(k_0, |\mathbf{r} - \mathbf{r}'|)$ is determined from the requirement that the overall functional must satisfy Eq. (5). The modifications proposed by Perrot,[21] Smargiassi and Madden,[30] and Wang et al.,[31] are similar to Eq. (8) in spirit and differ from Eq. (8) only in the explicitly nonlocal third term. One potential point of concern for functionals of this type comes from an upper bound for $T_s[n]$ first conjectured by Lieb:[32] $T_s[n] \le T_{\mathrm{vW}}[n] + T_{\mathrm{TF}}[n]$. If the third term in Eq. (8) evaluates to a positive number, the bound is violated. Like $T_{\mathrm{WT}}[n]$, each of these functionals depends on a fixed reference density, which is usually chosen to be the average density of the system. For this reason, the functionals in this category are most applicable for extended systems and their respective nonlocal terms may be evaluated with (quasi-)linear-scaling computational effort. However, if applied to systems with strongly varying electron densities, these functionals may become variationally unstable.[33] Finally, Wang and Teter,[22] as well as Foley and Madden,[34] developed generalizations of the same basic approach that return the exact result up to an additional order in perturbation theory for a weakly varying free-electron gas.

A more significant modification was proposed by Wang, Govind, and Carter (WGC).[35] The WGC functional is given by

$$T_{\mathrm{WGC}}[n] = T_{\mathrm{vW}}[n] + T_{\mathrm{TF}}[n]$$
$$+ \int \mathrm{d}\mathbf{r} \int \mathrm{d}\mathbf{r}'\, n^\alpha(\mathbf{r})w\big(k_0^\gamma(\mathbf{r}, \mathbf{r}'), |\mathbf{r} - \mathbf{r}'|\big)n^\beta(\mathbf{r}) \quad ,$$
$$(9)$$

where $\{\alpha, \beta\} = \{5/6 \pm \sqrt{5}/6\}$ and, importantly, k_0 is replaced with the two-point Fermi-wave vector $k_0^\gamma(\mathbf{r}, \mathbf{r}')$ that injects additional density dependence into the nonlocal term. This change is intended to improve the treatment of systems with more rapidly varying densities but does complicate the implementation of the functional. To regain quasi-linear scaling, WGC developed an approximate implementation of their nonlocal term that relies on a Taylor expansion about a fixed reference density. Subsequent work examined the WGC integral kernel in more detail[36] and also attempted to improve the performance of the WGC functional for nonmetallic systems.[37]

3. Additional nonlocal kinetic energy density functionals

a. Nonlocal functionals for the kinetic potential

The term kinetic potential refers to the functional derivative of the KEDF, $v_{T_s}(\mathbf{r}) = \delta T_s[n]/\delta n(\mathbf{r})$. There is some evidence for the contention that $v_{T_s}(\mathbf{r})$ is less severely nonlocal as a functional of the electron density than $T_s[n]$, and therefore more amenable to approximation. Moreover, for a given $v_{T_s}(\mathbf{r})$, there exist a variety of integration techniques for regaining the full kinetic energy. Motivated by these considerations, Chai and Weeks[38,39] developed a series of functionals for the kinetic potential, including two nonlocal functionals that are similar in spirit to those discussed in the previous section. Chai and Weeks initially tested their nonlocal functionals for atoms and ions. Later, in conjunction with coauthors,[40] they applied (quasi-)linear-scaling versions of their functionals to solid-state systems, obtaining very good results for Al and medium-quality results for Si.

b. The Huang–Carter functional

Electrons in a metal may conceivably be excited into states with energies infinitesimally higher than the Fermi level, whereas electrons in insulators must surmount a finite energy gap to access higher-energy states. This fact fundamentally alters the character of the density–density response function for insulators. The Lindhard response function discussed above, $\chi_0(\mathbf{k})$, has the limiting behavior of a metal. In view of these observations, Huang and Carter (HC) developed a KEDF that incorporates the expected limiting form of the response function for insulators.[41] Specifically, HC devised a modified version of the Wang–Teter functional[22] to increase its applicability for gapped materials. These modifications increase the computational prefactor for the HC functional by one or two orders of magnitude over the Wang–Teter and WGC functionals. The resulting KEDF requires specification of two adjustable parameters; however, by comparing OFDFT results with KSDFT data, HC determined a single pair of values for these parameters for computing the bulk properties of a range of tetrahedrally bonded semiconductors. Subsequent work explored the feasibility of studying molecules with the HC functional.[42]

c. Nonlocal functionals based on density decomposition

This subsection introduces a strategy for improving the calculation of $T_s[n]$ when $n(\mathbf{r})$ has localized features arising from, for example, covalent bonds or d electrons in transition metals. Each of the relevant studies employs a density decomposition of the form $n(\mathbf{r}) = n_{\text{del}}(\mathbf{r}) + n_{\text{loc}}(\mathbf{r})$, where $n_{\text{del}}(\mathbf{r})$ and $n_{\text{loc}}(\mathbf{r})$ refer to, respectively, delocalized and localized contributions to the total electron density. The density—decomposition technique involves (re-)writing $T_s[n]$ as

$$T_s[n] = T_s[n_{\text{del}}] + T_s[n_{\text{loc}}] \\ + (T_s[n] - T_s[n_{\text{del}}] - T_s[n_{\text{loc}}]) \quad , \quad (10)$$

where the term in parentheses represents an interaction energy that is frequently referred to as the nonadditive kinetic energy.[43] The nonlocal functionals discussed above are appropriate for computing $T_s[n_{\text{del}}]$ but less satisfactory for terms involving the localized density. Finally, it is clear from Eq. (10) that the density decomposition philosophy shares much in common with various embedding theories.[43–46]

The first attempt at density-decomposition-based OFDFT was made by Huang and Carter,[47] who used the HC functional[41] for $T_s[n_{\text{del}}]$; subsequent work by Xia and Carter[48,49] used the WGC functional[35] for $T_s[n_{\text{del}}]$, in part to improve computational efficiency. In all cases, simpler functionals of the form $aT_{\text{TF}}[n] + bT_{\text{vW}}[n]$ were used for terms involving the localized density, in the absence of better choices. In addition, Huang and Carter took the simplifying step of fixing $n_{\text{loc}}(\mathbf{r})$ after making an initial decomposition based on the character of $n(\mathbf{r})$ for a single atom. Xia and Carter generalized this approach by allowing $n_{\text{loc}}(\mathbf{r})$ to vary self consistently over the course of a calculation, employing a simple probe to assess the degree of localization at any given point. The initial Xia-Carter strategy required an external self consistency loop,[48] while a more recent version does not.[49]

d. The enhanced-vW functional

As discussed above, the vW functional returns the exact kinetic energy for single-orbital systems. For this reason, it is reasonable to expect that $T_{\text{vW}}[n]$ will play an especially important role in the analysis of more general systems with localized electrons—especially when the localized features are dominated by a single orbital. This observation motivates the enhanced-vW (EvW) functional proposed by Shin and Carter,[50] which is based on the earlier WGC functional[35] and retains the computational efficiency of the latter. The EvW functional assesses the degree of localization present in an electron density and, when $n(\mathbf{r})$ is dominated by localized features, enhances the relative contribution of the vW term within the overall WGC functional. Specifically, the EvW functional has the following structure

$$T_{\text{EvW}}[n] = (1+A)T_{\text{vW}}[n] + \left(1 - \frac{A}{2}\right)\left(T_{\text{TF}}[n] + T_{\text{WGC}}^{\text{nl}}[n]\right) \quad ,$$

$$(11)$$

where $T_{\mathrm{WGC}}^{\mathrm{nl}}[n]$ refers to the nonlocal term from the WGC functional. The enhancement factor A is given the simple form

$$A = k \left(\frac{n_{\max} - n_{\mathrm{avg}}}{n_{\mathrm{avg}}} \right)^2 \quad , \quad (12)$$

where k is an adjustable, material-dependent parameter, and $n_{\max}$ and n_{avg} refer to, respectively, characteristic maximum and average densities for the system under study. The strategy for choosing $n_{\max}$ and n_{avg} is somewhat subtle but is described in the original paper. This overall philosophy, along with suitable choices for the parameter k, allows EvW to achieve reasonable agreement with KSDFT for III–V semiconductors and to properly describe both the metallic and semiconducting bulk phases of Si.

B. Local pseudopotentials

While all-electron OFDFT rests on a solid theoretical foundation, it is generally not the most expeditious choice from a computational perspective. In practice, a great majority of OFDFT calculations are conducted with the valence electron density alone, and rely on LPSs to represent the combined effect of core electrons and the nuclear potential. Common KSDFT techniques, such as nonlocal pseudopotentials (NLPSs) or the projector-augmented-wave[51] (PAW) approach, are inapplicable because the standard OFDFT lacks orbital information (although we refer the reader to Sec. IV for more discussion on this point).

Over time, the construction of LPSs has evolved in complexity and accuracy. Early OFDFT studies used LPSs with simple analytic forms that were parameterized based on data from experiments or from more accurate electronic structure calculations.[22,52] While this approach is marked by concerns regarding transferability, it remains in use today, sometimes with great success.[53,54] In principle, LPSs obtained from first principles are applicable in a much wider range of environments, and several protocols have appeared in the literature. Each of the methods for constructing first-principles LPSs has the same goal—to match the electron density (or other properties) obtained with an LPS calculation to that of a KSDFT-NLPS/PAW benchmark—but the methods differ in the choice of reference environment.

1. Atomic local pseudopotentials

Atomic LPSs are based on the KSDFT valence electron density for free atoms and have been successfully applied to the group IV elements Si, Ge, and Sn.[55] However, even when used in KSDFT calculations, atomic LPS results can be insufficiently accurate for the

calculation of atomic excitation energies, as well as the band structures of solids. A major drawback is a lack of transferability and insufficient accuracy for crystal applications.[56] Finally, Mi et al. recently proposed a related strategy that develops LPSs directly from first principles norm-conserving pseudopotentials.[56]

2. Bulk-derived local pseudopotentials

Bulk-derived LPSs (BLPSs) are based on KSDFT valence electron densities derived from one or more bulk crystalline environments. The first BLPSs were obtained by requiring that an OFDFT calculation (performed with a particular KEDF) reproduces exactly a reference density from a KSDFT calculation; as a result, these BLPSs were KEDF dependent.[57] More recent work has emphasized KEDF-independent BLPSs, which are constructed from KSDFT calculations alone and are therefore expected to be more transferable.[56,58,59] BLPSs have been successfully applied to numerous solid-state calculations on a variety of materials,[42,56,59] including Li, Mg, Al, Ga, In, P, As, Sb, and Si, as well as the III–V semiconductors[41,48,50] GaP, GaAs, GaSb, InP, InAs, and InSb. Additionally, liquid Li and the Li melting temperature have been successfully investigated with a BLPS.[60,61] However, inaccuracies arise for liquid phases of more complex systems.

3. Neutral pseudoatom method

The neutral pseudoatom (NPA) method was first introduced by Ziman[62] in 1964 and later developed by Dagens[63] for the study of metallic Li and Na. It is based on a representation of the valence-electron density of an atom in a positive background of a uniform electron gas. Anta and Madden[64] used this reference system to develop KEDF-dependent ab initio LPSs, and such LPSs have proven useful for OFDFT studies of liquid metals.[65] However, because the NPA is constructed from the discrete environment of an isolated atom, inaccuracies can appear for liquids, where the atom is surrounded by others in a disordered array. One successful modification that involves a force-matching procedure was introduced by del Rio and González.[66] In this procedure, the initial NPA LPS is modified by the addition of Gaussian functions to minimize the difference in the forces calculated with a NLPS-KSDFT calculation and the NPA LPS-OFDFT calculation for a given liquid configuration. The liquid sample used for the NLPS-KSDFT benchmark calculation must be small ($\sim$100 atoms) and simulated for a short time ($\sim$10 ps). The force-matching modification has been applied successfully to the study of Be, Ca, and Ba.

4. Globally-optimized local pseudopotentials

Recently introduced by three of the authors,[67] the globally-optimized LPS (goLPS) method is the first

construction procedure explicitly designed to represent both solid and liquid phases correctly, and therefore will be especially useful for multi-phase simulations. The goLPS strategy can also be used to improve a given solid or liquid LPS and, thus far, goLPSs have been constructed successfully for Li, Ca, and Ga.

C. Algorithms and implementation details

Several OFDFT codes have been described in detail in the literature.[68–75] In this section, we seek to answer the following questions: (i) what capabilities and level of performance can a researcher expect from an OFDFT code; (ii) how have the major algorithmic hurdles been overcome thus far; and (iii) what future algorithmic challenges require attention? The objective and capabilities of OFDFT are very similar to those of KSDFT: both theories endeavor to find, for a given arrangement of atoms and boundary conditions, the ground-state energy and the self-consistent solution for the electron density. While there are technical differences between OFDFT and KSDFT implementations—and, in fact, within the two paradigms separately—the actual computation of static and dynamic properties is typically conducted in a similar fashion. Physical properties are computed from, say, converged electron densities or perhaps extracted from repeated simulations of the same system, each with a slightly modified arrangement of atoms. Because OFDFT codes can be made to scale with (quasi-)linear computational complexity as additional atoms are included in a simulation,[68,76] they are especially appealing for study of phenomena involving large numbers of atoms and/or long time scales. In what follows, we first establish what is required to achieve (quasi-)linear scaling for a single iteration of a self-consistency cycle. Subsequently, we discuss the reduction of absolute evaluation times.

The most basic feature that differentiates OFDFT implementations is the choice of basis set for representing the electron density. Planewave representations (or, almost equivalently, Cartesian grids in real space with equidistant spacing) have been used traditionally in conjunction with judicious use of Fast Fourier Transforms (FFT)s.[68–71,77] Specifically, FFT-assisted convolutions are useful for evaluating many nonlocal KEDF terms, reducing the quadratic scaling of naïve implementations to quasi-linear scaling. Similarly, the electron–electron repulsion energy $E_H[n]$ may be obtained almost trivially with a pair of FFTs. The local density approximation for the exchange-correlation term, $E_{xc}[n]$ is straightforward to evaluate without FFTs, and the extra gradient information required by generalized gradient approximations for $E_{xc}[n]$ may also be computed with efficient, FFT-assisted techniques. More care is required for the electron-ion and ion–ion terms, which scale quadratically in naïve implementations. For the ion–ion

term, an Ewald summation is frequently required; our code, PROFESS,[69–71] achieves quasi-linear scaling with a cardinal B-spline implementation[78] of the particle mesh Ewald method. The ion—electron term may also be evaluated with quasi-linear scaling using a B-spline approach for computing the structure factor.[77,79]

FFT-based implementations are known to exhibit limited parallel scalability with standard FFT libraries.[80] Because FFTs incur the majority of the communications overhead in an FFT-based OFDFT code—by contrast, integrations over the full grid are nondemanding and occur less often—FFT scalability determines the overall scalability of such codes. However, for many systems of interest, the absolute speed of FFT-based implementations is sufficient even with a limited number of processors; FFTs become a bottleneck only for extremely large systems also requiring very fast (and hence massively parallel) evaluations. A recent demonstration of petascaling OFDFT[81] overcomes parallelization limitations by partitioning energy functionals into short- and long-ranged contributions and then employing a multi-grid approach where smooth contributions are evaluated on a coarse global grid while more rapidly varying contributions are evaluated with local "small-box" FFTs. Such techniques can be used for the explicit quantum-mechanical study of millions of atoms. Another approach that is applicable for simulations of medium to large systems (presently, up to tens of thousands of atoms) is to make use of compute accelerators such as GPUs. Even though FFTs are a task not ideally suited for GPUs and hence currently unable to extract even close to theoretical peak performance out of GPU hardware, we find the absolute performance of accelerated KEDF implementations to be excellent.[82] Currently, constraints for GPU-accelerated OFDFT arise because of memory limitations on the accelerators; these limitations begin to appear in the realm of hundreds of grid points per Cartesian dimension.

Purely real-space representations of the electron density, in contrast with FFT-based implementations, trade a small complexity prefactor and code simplicity for better fundamental parallel scalability. Large improvements have been made in recent years to reduce the high prefactor of real-space implementatons.[75,83–85] An important first step is to develop an evaluation strategy for nonlocal terms that does not depend on operations in the reciprocal space. In particular, long-range electrostatic interactions, including Poisson terms,[85] can be computed from a local variational problem. Similarly, the nonlocal integral kernels appearing in the WGC KEDF can be reformulated as a series of Helmholtz equations in real space.[86] Results discussed in the literature show that such real-space algorithms can be used to simulate tens of thousands of atoms with full atomic resolution, and millions using coarse-graining techniques.[87]

Next, we note one important implementation detail pertaining to the use of preconditioners and electron density optimization approaches in OFDFT. The computational prefactor for OFDFT calculations depends on the number of iterations required to obtain a converged total energy and electron density. Some insight has been gained on preconditioning strategies for bulk systems;[88] however, possibilities for development remain, particularly regarding transferable preconditioners and local optimization procedures applicable to finite systems.

While we emphasize OFDFT in this review, other algorithmic ingredients such as techniques for geometry optimization and MD propagators are shared with KSDFT approaches. The typical performance of OFDFT codes allows one to study systems with dynamic exploration methods such as MD and also makes OFDFT an attractive ingredient for multi-scale and quasi-continuum simulations.[89–91] Future integration of OFDFT with techniques beyond these, such as advanced sampling and exploration techniques, will be straightforward and should prove to be scientifically beneficial.

III. MATERIALS RESEARCH WITH OFDFT

This section reviews contributions of OFDFT to the understanding of a diverse range of materials, including solids, liquids, and multi-phase systems. Each of the studies described below was conducted with OFDFT calculations, sometimes in conjunction with other methods. We eschew discussion of most computational details but provide references for the interested reader. Unfortunately, quantitative agreement between OFDFT and standard KSDFT varies on a case-by-case basis and, for any given material, one must verify that the two theories give the same result for small systems before proceeding to larger systems accessible only with OFDFT. For this reason, the studies that we discuss typically include such a validation step to promote confidence in the results. In general—at least with the nonlocal functionals described above—quantitative agreement between OFDFT and KSDFT (and/or experimental data) is achieved for light metals and their alloys. Useful quantitative results may also be obtained for other materials but, at present, more caution is warranted.

A. Solids

Bulk crystalline solids, particularly those without strongly correlated electrons, were among the earliest successes of both KSDFT and OFDFT.[92] For simple cases, such as a defect-free solid composed of a single element, simulations involving a few or tens of atoms subject to periodic boundary conditions are sufficient for determining physical properties such as equilibrium volumes, elastic behavior, and relative energies of

various crystalline phases—and the computational efficiency of OFDFT is generally unnecessary for such cases. However, analysis of alloy phases (e.g., high entropy alloys[93]) may require hundreds or even thousands of atoms. Moreover, the behavior of real solids is altered by defects and defect-driven phenomena, some of which—such as the nucleation and motion of dislocations, or diffusion along grain boundaries in a polycrystal—may affect thousands of atoms. Finally, other defects involve only a few atoms but occur in tiny concentrations, meaning that many-atom simulations are required for a realistic treatment. The following subsections explore these topics more in detail.

1. Solid alloys

The majority of OFDFT studies on crystalline alloys thus far have considered Mg–Al compounds. Both Al and Mg are abundant metals, and Mg–Al intermetallic compounds have high strength-to-weight ratios and other favorable mechanical properties. Moreover, one expects that OFDFT will be reasonably accurate for Mg–Al compounds of a wide range of compositions because the valence electrons are delocalized in both bulk Al and bulk Mg. Several roles for OFDFT calculations are illustrated below using examples drawn from a series of studies on Mg–Al alloys.[73,94–96] Perhaps the most important task is to assess the stability (or meta-stability) of a candidate compound, which is a multipart endeavor. A thorough stability analysis involves consideration of a compound's formation energy, elastic behavior (mechanical stability), and phonon spectra (dynamical stability).

The formation energy, E_f, is a useful first descriptor of structural stability: a negative E_f provides evidence for stability, whereas a positive E_f suggests that the compound is energetically unfavorable and may even decompose into secondary phases. Formation energies at zero Kelvin have been computed for a variety of Mg–Al compounds. Table I summaries the results of some of these calculations. For simplicity, Table I gives only a plus sign if the computed value of E_f is positive and a minus sign for negative E_fs, reflecting either a consensus in the literature or (in a few cases) the result that is expected to be the most accurate. We note that while most compounds presented in Table I have relatively small unit cells, the β'-Mg_2Al_3 phase considered by Das, Iyer, and Gavini[73] requires an 879 atom simulation. The three compounds in Table I listed in boldface type are found in the experimental Mg–Al phase diagram, with β'-Mg_2Al_3 among them.

The utility of OFDFT becomes more apparent for assessment of mechanical and, especially, dynamical stability. A compound's mechanical stability is closely related to its elastic behavior, and a mechanically stable

TABLE I. Summary of stability analyses performed on a variety of Mg–Al compounds. Those compounds which pass all three stability tests (described in the text) are expected to be at least meta-stable. The compounds listed in boldface type are present in the experimental phase diagram; each of these compounds passes all three stability tests.

Composition	Identifier	Primitive cell atoms	Formation energy (E_f)	Mechanically stable?	Dynamically stable?	References
MgAl$_3$	β″	4	−	. . .	. . .	73 and 94
MgAl$_2$	. . .	12	+	y	y	95
∼Mg$_2$Al$_3$	β″	879	−	. . .	. . .	73
Mg$_{23}$Al$_{30}$	. . .	53	−	y	y	73 and 95
Mg$_{13}$Al$_{14}$	. . .	27	+	n	n	73 and 95
Mg$_{17}$Al$_{12}$	. . .	29	−	y	y	73 and 95
	D0$_{19}$	8	−^{a}	y	y	96
Mg$_3$Al	L1$_2$	4	−^{a}	y	y	96
	D0$_3$	4	+	. . .	n	96

^{a}KSDFT calculations and evaluation of the zero point energy were required to resolve ambiguities in the formation energies for these compounds.

compound in its ground state will resist any applied strain. One verifies mechanical stability by ensuring that a compound's stiffness tensor is positive definite; if not, the compound will be mechanically unstable. These elastic properties are synthesized from many simulations of the same cell, each perturbed by a small strain. Table I indicates those compounds which pass the mechanical stability test, when the data are available.

Dynamical stability is assessed from the crystal's phonon spectra: imaginary phonon modes, when observed, imply that the compound is dynamically unstable. The simulations that are used to generate phonon spectra require more atoms than are in the simple unit cell; for example, the phonon spectra calculations for Mg$_{23}$Al$_{30}$, another compound in the experimental phase diagram, involved simulations of 1431 atoms.[95] Those compounds which pass the dynamical stability test are also reported in Table I. Phonon spectra, once computed, enable determination of thermodynamic properties such as the temperature-dependent formation energy, heat capacity, and thermal expansion coefficient.

A recent study by Zhuang, Chen, and Carter[95] illustrates an additional use for OFDFT in the study of alloys: computational discovery of new materials. This study used OFDFT to rapidly screen 101 Mg–Al compounds and used these results in conjunction with a cluster expansion model to explore 5675 additional compounds. After narrowing the field to three compounds, each with composition Mg$_3$Al, Zhuang, Chen, and Carter then used KSDFT calculations to predict a new meta-stable compound (D0$_{19}$ Mg$_3$Al) that is expected to exhibit greater stability and superior ductility when compared with other candidate structures of the same composition.

While the majority of OFDFT studies on solid alloys have considered Al and Mg, there are a growing number of examples involving other materials. For example, Shin and Carter have explored plasticity in BCC Mg–Li alloys.[53] Improvements in KEDFs have also spurred new applications, including studies of crystalline Li–Si alloys[97] and amorphous Li–Si alloys.[49]

2. Defects in solids

The existence and behavior of defects in a crystalline solid can alter its properties dramatically, and OFDFT enables realistic simulations of such defects that are challenging or impossible to conduct with most other methods. One can employ several distinct strategies for modeling a defect within an extended system. Codes that employ periodic boundary conditions model a periodic array of defects, and the user increases the size of the simulation cell until interactions between the defects become negligible. Bulk Dirichlet boundary conditions are another option, where the boundaries are fixed in accordance with the electronic structure of the bulk material. This choice models a true isolated defect but, again, requires the user to increase the computational domain until the property of interest reaches a converged value.

a. Vacancies and vacancy clusters

A useful starting point is a single, isolated vacancy within a face-centered cubic (FCC) Al lattice. The formation energy E_{vf} of this defect at zero Kelvin has been computed with OFDFT by several authors.[31,35,73,98–100] When the defect is modeled with periodic boundary conditions, the value of the formation energy converges for simulations of 108–256 atoms.[73,98] However, larger simulations of at least 864 atoms are required for convergence of the electronic structure,[73] which exhibits meaningful perturbations from its bulk character over distances of at least five lattice units from the defect. In contrast, when the isolated defect is studied with bulk Dirichlet boundary conditions, neither E_{vf} nor the electronic structure converge until the cell size reaches 864 atoms.[73] In addition to the vacancy formation energy, Ho et al. also examine the diffusion kinetics of vacancy motion.[98] Finally, in part because the aggregation of vacancies may lead to larger defects such as voids, several authors have investigated the behavior of vacancy clusters[84,98,99] including di-vacancies,

tri-vacancies, tetra-vacancies, and one example involving a 19-vacancy cluster.[84]

b. Dislocation nucleation, structure, and motion

Dislocations are among the most important many-atom defects because dislocation nucleation, structure, and motion, as well as interactions between dislocations and other defects such as grain boundaries, strongly influence the plastic deformation behavior of metals. In the immediate neighborhood of a dislocation, the electronic structure is disrupted rather severely from its bulk character and so a simulation approach that adheres to the appropriate physics is essential. Away from its core region, a dislocation generates a long-ranged elastic strain field that is also an important part of the overall effect. A simulation tool for dislocations must be able to faithfully capture both phenomena.

The initial series of OFDFT studies in this area examined the onset of plasticity via dislocation nucleation developing at surfaces during nanoindentation.[89,101–103] (Strictly, the works described in this paragraph were conducted by coupling OFDFT with a local quasi-continuum method,[104–106] but we will not elaborate on the distinction here.[107]) The first papers in this series[89,101] used a simulated spherical indenter of 750 nm to probe Al surfaces, highlighting the importance of using indenters with experimentally relevant sizes. Subsequent studies made similar investigations for an Al_3Mg alloy[102] and an Al thin film with Mg impurities.[103] More force was required to indent the Al_3Mg alloy than was required to indent Al, which was an expected result; however, in the Al thin film case, both hardening and softening were observed, depending on the local distribution of Mg impurities.

Multiphysics strategies that couple OFDFT with classical molecular mechanics simulations have also been used for the study of dislocations. Choly et al. applied such an approach to examine the core structure of a screw dislocation in Al.[90] Zhang and Lu, using a similar method, investigated the diffusion of a Si atom along an edge dislocation in Al.[108]

Finally, OFDFT has also enabled direct, atomic-scale study of the structure of edge and screw dislocations in both Al[109–111] and Mg.[112] These simulations generally required at least 1500–3000 atoms, and the authors observed perturbations in the electronic structure that extend for tens of Ångstroms from the main defect, or more. Follow-up studies considered the motion of dislocations in both Al[113] and Mg,[114] as well as in Mg–Li alloys.[53] Fig. 1 shows the energy barrier to motion for both edge and screw dislocations in Al. Finally, a recent study examined a possible originating mechanism for dislocations in bulk Al, which involves the collapse of a 19-atom cluster into a dislocation loop.[84]
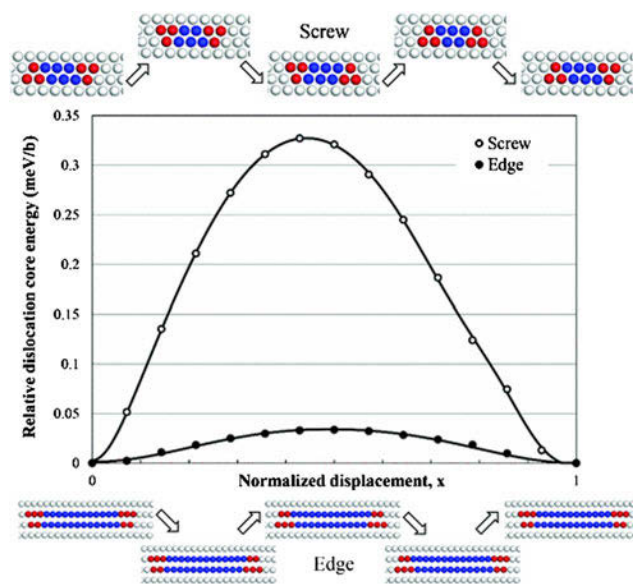

FIG. 1. Variation of dislocation core energies for screw and edge dislocations in aluminum as a function of the normalized displacement x traveled by the dislocation core. The energy unit is meV/b where b is the Burgers vector. Insets show corresponding atomic configurations of the screw (upper inset) and the edge (lower inset) dislocation cores along the minimum energy path. Gray, blue, and red spheres indicate atoms locally in face-centered cubic, hexagonal close-packed, and unknown crystal structures, respectively. Reproduced figure with permission from Shin and Carter, *Phys. Rev. B* **88**, 064106 (2013). Copyright 2017 by the American Physical Society.

c. Other large-scale defects

A few OFDFT studies have considered other large-scale defects in solids. For example, Watson and Madden used OFDFT-MD to simulate grain boundary migration in crystalline sodium.[115] Hung and Carter explored ductile crack propagation in Al,[116] contrasting predictions made by OFDFT with predictions made using a classical potential. Finally, a recent study by Chen et al. determined the optimized structure for a polycrystalline Li sample consisting of eight grains, each with a radius of approximately 60 Å, and nearly 400,000 atoms.[81]

d. Nanoscale materials

The properties of nanostructured solids can differ dramatically from their bulk counterparts and OFDFT has been used to investigate several categories of nanoscale materials. For example, Watson and Carter considered an array of Al quantum dots,[68] investigating the effect of separation distance on the decay of the electron density in the vacuum region between adjacent quantum dots. A number of studies—see Ref. 117 for a summary—have considered alkali metal clusters and alkali metal alloy clusters. OFDFT has also been used to study the mechanical properties of Al nanowires,[118,119] including elastic properties and mechanisms for tensile yielding.

We expect studies of this kind to become increasingly common as OFDFT advances in maturity.

B. Liquids

This section reviews the application of OFDFT-MD to liquid metals and alloys. In principle, OFDFT allows for a realistic treatment of liquids because large samples may be considered for long simulation times. The most success so far has been achieved for simple (*s*- and *p*-bonded) metals because these systems may be treated accurately by available KEDFs and LPSs due to their nearly-free-electron-like nature.

1. Bulk liquid metals

Over the last fifteen years, the OFDFT-MD method has been applied to describe a wide range of static, dynamic, and electronic properties of simple liquid metals. The study of time-dependent phenomena usually requires long simulations involving thousands, or tens of thousands, of configurations to avoid problems associated with noise and limited correlation time. OFDFT-MD is well suited for this task, while KSDFT-MD simulations of liquids are usually restricted almost entirely to the study of static properties.

s- and *p*-bonded liquid metals have been studied extensively with OFDFT, beginning with the pioneering work of Madden and coworkers on the static structure of liquid Na, Mg, and Al.[120,121] Others considered the single-particle dynamic properties of liquid Li.[60,64] In addition, OFDFT-MD has been used to study the static and dynamic properties of liquid Cs[28] at several points along the liquid–vapor coexistence line. The first study on collective dynamic properties of liquid alkaline-earth metals occurred in 2009; in this work, a special feature was observed in the static structure factor, $S(q)$, of liquid Mg.[122] This special feature is a shoulder on the second peak of $S(q)$, which is related to the capacity of the liquid metal to undercool. Subsequent studies on Be, Ca, and Ba[66] revealed the same feature, making it a common property of liquid alkaline-earth metals.

Of the *p*-bonded liquid metals, Al has been studied most often because of its nearly-free-electron-like nature. Work by González et al.[29,123] considered the static and dynamic properties of Al at various temperatures, and warm dense Al was recently studied by White et al.[124] and Sjostrom and Daligault.[125] White et al. highlighted the inability of classical MD to fully capture quantum effects in cases where electron oscillations couple with ion-acoustic modes, whereas OFDFT includes these effects by continuously updating the electronic response. Sjostrom and Daligault compared OFDFT results to KSDFT results, obtaining excellent agreement for several properties, and were able to use OFDFT to study much higher temperatures than those accessible with KSDFT

because the computational cost of their method does not increase with temperature.

OFDFT-MD studies on complex liquid metals have been performed successfully for liquid Ga[126] and liquid Si under pressure.[127,128] In both cases, a peculiar shoulder in the main peak of $S(q)$ was observed at several temperatures. In addition, covalent-like bonding present in both liquid Ga and liquid Si was studied with OFDFT; Fig. 2 shows a comparison between OFDFT- and KSDFT-derived density profiles for liquid Ga, and reasonable agreement is apparent.

2. Bulk liquid metal alloys

The field of liquid metal alloys was stimulated by the results of a classical MD simulation of liquid Li_4Pb by Jacucci et al.,[129] who observed a new, high-frequency mode supported by the Li atoms only and named it the fast-sound mode. The dispersion curve for pure liquid metals, which contains information about the propagation of collective density fluctuations, has only one branch that begins in the hydrodynamic regime corresponding to very small wave vectors (q) and extends to higher wave vectors. (The slope of the dispersion curve for $q \rightarrow 0$ is the adiabatic sound velocity.) In contrast, the dispersion curve for liquid metal alloys has one branch in the hydrodynamic regime and then splits into two branches as the wave vector increases. The two branches correspond to two separate modes, the fast-sound mode and the slow-sound mode, and the bifurcation signals the onset of a dynamic decoupling between the two types of particles. Accordingly, the fast mode is expected to resemble the individual dispersion relation of the corresponding light particle fluid.[130,131] The OFDFT-MD method has been applied to several liquid metal alloys (Na–Cs,[132] Li–Na,[133] and Ga–In[117]) to gain insight into the existence and properties of the collective excitations in these liquids as well as to study the fast-sound mode. Homo-coordinating tendencies are observed for Na–Cs and Li–Na, where each particle tends to be surrounded by particles of the same type, but the segregating tendency lessens as temperature increases.

3. Liquid metal surfaces

The study of the structure of free liquid surfaces has attracted much theoretical and experimental attention, with a strong emphasis on the possible existence of liquid surface layers. It had long been believed that the change in the ion density when crossing from the liquid into the vapor is monotonic.[134] X-ray measurements on several nonmetallic liquids[135] revealed density profiles that decay smoothly and monotonically from the high-density bulk liquid to the low-density vapor. However, oscillatory density profiles extending several atomic diameters into
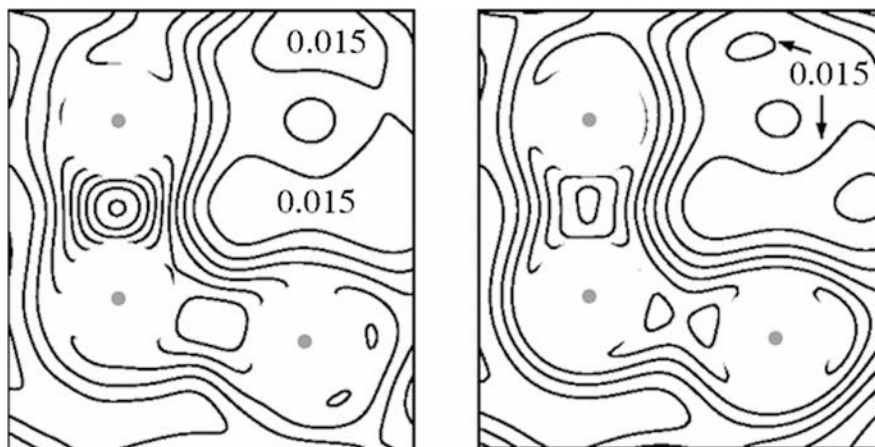
FIG. 2. Electron density for a triplet of Ga atoms at 373 K obtained with OFDFT (left) and KSDFT (right). The contour lines are plotted for values of the density equal to 0.010 electrons/a.u., which corresponds to the minimum inside the peanut-shaped line in the right part of the KSDFT data, and then for increments of 0.005 electrons/a.u. Contour lines within the core radius ($\approx$0.75 Å) of each atom have been deleted because the pseudodensity within the core has no physical meaning. Reproduced figure with permission from González, González, and Stott, *Phys. Rev. B* **77**, 014207 (2008). Copyright 2017 by the American Physical Society.

the bulk liquid were observed with X-ray measurements of several liquid metals (e.g., Ga[136]) and alloys (e.g., In–Ga[137]). This feature, which suggests a layering parallel to the interface, is of great interest. Given that metallic bonding is very different from that of molecular fluids, it is not surprising that nonmonotonic oscillations in the density are observed for the former in contrast to the latter.

In a metallic system, the nature of the interactions between ions changes drastically across the liquid–vapor interface. The computational demands of the KSDFT-MD method have restricted its application to only two systems, l-Si and l-Na,[138,139] but OFDFT-MD has proven capable of treating many more liquid metal and binary alloy surfaces. Work on Li and Na liquid surfaces with OFDFT-MD,[140] for example, clearly revealed the surface layering phenomenon. Subsequently, liquid surfaces of more complex elements (K, Rb, Cs, Mg, Ba, Al, Tl, Si, Ga, and In) were also studied, which led to the verification of a scaling relationship between the wave length of ionic oscillations and the radii of the associated Wigner–Seitz spheres.[141,142] In addition, OFDFT-derived estimates for the reflectivity agreed well with X-ray measurements.[162,163]

First-principles MD studies of liquid metal alloy surfaces have only been possible with OFDFT-MD. So far, the work has been restricted to the Ga–In alloy at the eutectic point[142] and several concentrations of the interalkali alloys Na–K, Na–Cs, and Li–Na.[143,144] An interesting segregation tendency has been observed and attributed to differing surface tensions between the constituents of the alloy; the result is a high concentration at the surface of the compound with the lowest surface tension, as would be expected thermodynamically. This phenomenon is clearly seen in Fig. 3, which shows the density profile for a liquid
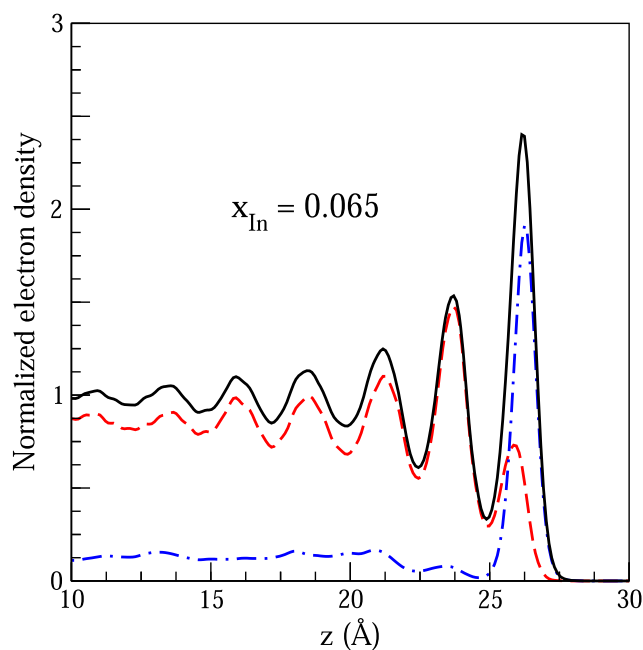

FIG. 3. Total electron density, normalized to the bulk value of the slab, for liquid $Ga_{0.935}In_{0.065}$ (thick continuous line). The dashed and dash-dotted lines are the Ga and In contributions, respectively, to the total electron density. Received by private communication from the authors of Ref. 142, and used with permission.

surface of GaIn, as well as profiles for the individual Ga and In contributions. Specifically, the normalized contribution of In increases dramatically at the surface on the right hand side of Fig. 3.

C. Multi-phase systems

A great number of technological and physical processes, such as soldering, lubrication, and crystal growth

or melting, involve more than one phase of matter. Long simulation times are required to model these systems, along with accurate representations of all phases and phase transitions. OFDFT-MD is an alternative to classical MD that provides (in principle) a more accurate description of the system, while retaining manageable computational expense.

1. Solid-liquid interfaces

Early studies of solid–liquid interfaces regarded the solid as a continuous system and modeled its interaction with the liquid using a potential that depended only on the distance from the wall. However, a truly accurate description of interfaces between phases requires an atomic-scale description and, in particular, a proper description of the forces between atoms. We concentrate first on studies related to the static and dynamic properties at solid–liquid interfaces and then comment more extensively on melting temperature calculations in the next subsection.

The solid–liquid interface most studied with OFDFT-MD has been that of Al. The first such simulation was reported in 2000 by Jesson and Madden,[145] who studied a solid Al surface in equilibrium with liquid Al. However, that study predicted a melting temperature that was much lower than experiment, suggesting deficiencies in the KEDF as well as in the LPS. Later work by González and González[146] examined liquid Al at 1000 K in contact with three different orientations of FCC Al: the (100), (110), and (111) surfaces. Interestingly, results differed depending on orientation. While in contact with the (100) surface, only the first layer in the liquid exhibited solid-like ordering, whereas the (111) surface induced a full solidification of the liquid which began to crystallize layer by layer.

In 2013, Aguado et al.[117] reported work on a solid–liquid interface between two dissimilar metals: liquid Li on solid Ca at a temperature of 470 K. Their periodic simulation cell contained vacuum, 576 Ca atoms arranged in 16 solid layers, and 2000 Li atoms in the liquid phase. An interesting phenomenon developed in the first liquid layer: the Li atoms in this layer followed one-dimensional trajectories along the channels on the exposed FCC (110) surface of Ca atoms.

2. Solid-liquid phase transitions

The calculation of a material's melting curve (i.e., how its melting temperature changes with pressure) is an arduous task for which several methods can be used, including the heat-until-melts scheme,[147] the (solid–liquid) coexistence approach,[148] and the Z-method.[149] The heat-until-melts method is subject to superheating;[147] it therefore yields an upper bound to the true melting temperature (the so-called mechanical melting temperature). OFDFT-MD simulations of the mechanical melting temperature of Li explored the effect of simulation cell size and concluded that at least 256 atoms must be included to achieve property convergence. The coexistence approach provides a more refined estimate of a material's melting temperature but requires a larger sample to accommodate simultaneous representation of both solid and liquid phases.[60]

The light alkali metals Li and Na undergo a series of phase transitions when subjected to compression, and this behavior is reflected in the associated melting line. In both cases, the melting curve reaches a maximum, and thereafter, as pressure is increased, the melting temperature decreases to a minimum before increasing again with a positive slope.[150,151] Only the melting curve of Na has been studied[152] in this capacity with OFDFT-MD, along with changes in the static, dynamic, and electronic properties of the liquid as pressure is increased. Analysis of the dynamic properties revealed that the increase in density due to pressurization increased the importance of interatomic collisions in controlling the dynamics of the system.

IV. OUTPOSTS ON THE OFDFT FRONTIER

This section contains brief discussions of additional topics that, while less directly connected to the application studies reviewed in the previous section, are nonetheless at the forefront of OFDFT research. The range of topics includes "new approaches to old ideas,"[4] as well as rather serious departures from the usual LPS approach.

A. Recent advances in single-point kinetic energy density functionals

Single-point functionals of the electron density have the general form $F[n] = \int d\mathbf{r}\, f(n(\mathbf{r}), \nabla n(\mathbf{r}), \ldots)$, and are evaluated with one, single integral. In contrast, aside from $T_{TF}[n]$ and $T_{vW}[n]$, the KEDFs discussed in Sec. II are two-point, nonlocal functionals; their evaluation requires two integrals. The relative simplicity of single-point functionals makes them advantageous from a computational standpoint. While, historically, single-point approximations for $T_s[n]$ have been insufficiently accurate for reliable, self-consistent OFDFT calculations on solids and liquids, progress in this subfield has accelerated recently.

There are at least three scenarios—aside from the self-consistent OFDFT calculations at low temperatures that we have emphasized thus far—in which single-point functionals have flourished. First, at high temperatures, such as those in the warm dense matter[9] regime straddling condensed matter physics and plasma physics, one typically observes smoothing in sharp quantum features that are present in the $T \to 0$ limit. This phenomenon

eases in some ways (and complicates in others) the challenge of determining OF approximations for the noninteracting free energy functional. Second, subsystem DFT[10,11] and various embedding approaches employ OF approximations for the non-additive kinetic energy;[43,45] fortuitous error cancellation and the smaller magnitude of the nonadditive contribution compared with the full $T_s[n]$ can again simplify the task somewhat. Finally, recent advances in the design of exchange-correlation functionals have incorporated the non-interacting kinetic energy density as an ingredient, and OF approximations for this quantity have proven useful.[153,154]

Single-point approximations for $T_s[n]$ have a long history that, for the sake of brevity, we do not discuss here and instead refer to prior reviews.[1,4,6,15,16,155] Our rather modest aim is simply to direct the reader to a small number of the very latest advances in this category. Generally, single-point density functionals rely on the value of $n(\mathbf{r})$ at each point and a few other dimensionless ingredients such as the reduced gradient $|\nabla n|/(2(3\pi^2)^{1/3}n^{4/3})$ and the reduced Laplacian $\nabla^2 n/(4(3\pi^2)^{2/3}n^{5/3})$. Functional developers combine these ingredients based on a variety of overlapping philosophies. Perhaps the most fundamental approach is to posit a functional form that accords with the collection of exact constraints that the true functional has been determined to obey.[153,156–158] Investigations that analyze the behavior of local kinetic energy density are useful in this regard.[159–164] A related series of studies takes inspiration from the semiclassical limit of atoms as $Z \to \infty$[165–169] and another approach seeks to impose proper representation of atomic shell structure.[170] One can also incorporate exact solutions for simplified model systems such as the locally-linearized potential model[171,172] or the jellium-with-gap model[173]—or simply search for the best combination of ingredients with a brute force scan.[154] Lastly, we mention an intriguing approach that makes use of a new ingredient, the reduced Hartree potential, although this functional is not strictly a single-point functional.[174]

B. Angular-momentum-dependent OFDFT

Angular-momentum-dependent (AMD) OFDFT was conceived by Ke et al.[175,176] Recalling that OFDFT regards the electron density, $n(\mathbf{r})$, as the sole quantity to be varied, the primary innovation of AMD-OFDFT is the introduction of single particle density matrices that describe the system in regions of space immediately surrounding each nucleus. This partitioning of the system domain—atom-centered spheres stitched together by an interstitial region—is commonly referred to as a muffin-tin geometry. Outside any particular atom-centered sphere, the AMD-OFDFT approach describes the system with the electron density alone, as is the case for ordinary OFDFT.

In principle, the extra information encoded in the onsite density matrices provides a more complete description of the physical system and therefore should enable more accurate calculation of the system energy. Importantly, one anticipates improvements over regular OFDFT for both kinetic energy and potential energy terms. Improvement for the potential energy is possible because the formalism is no longer restricted to LPSs and may instead treat electrons with different angular momenta differently, as is usually done with KSDFT.

The original articles by Ke et al.[175,176] demonstrated the validity of such an approach by showing that it could be used to compute bulk properties of the transition metal Ti. The localized d electrons in these materials typically preclude any successful application of OFDFT. However, this proof-of-principle work utilized a parameter fitting step that simplifies the overall formalism but reduces transferability. Efforts to overcome these limitations are ongoing.

C. OFDFT implementation with the PAW method

The final example[74] harnesses the PAW method,[51] which is well-established for KSDFT, in an OFDFT context. Applying the oft-used technique of interpreting the square root of the electron density as a pseudo-orbital, the authors reformulate the OFDFT problem so that it can be described by an effective Schrödinger equation for a model system. From there, they employ the PAW decomposition to conduct efficient all-electron, frozen-core calculations with OFDFT. When the same semi-local OFDFT functionals are used in both cases, the authors demonstrate their method agrees well with results obtained from more expensive, explicitly all-electron simulations. However, agreement with KSDFT is less satisfactory unless a parameter fitting step is used. Unfortunately, it is not immediately clear how to combine this general approach with the more accurate, nonlocal approximations for $T_s[n]$.

V. CONCLUDING REMARKS

Over recent decades, OFDFT has contributed meaningfully to the field of materials research by enabling direct, quantum-mechanical simulations of many-atom systems that would be otherwise impractical or impossible. Simulations involving thousands of atoms are now routine, and million-atom simulations are achievable. While early work emphasized main group metals with nearly-free-electron-like character, more recent advances provide satisfactory results for a wider portion of the periodic table, including many semiconductors. Ongoing efforts aim to overcome the challenges associated with strongly localized electrons. Innovations in theory and practice are occurring steadily, and we expect this trend to continue.

ACKNOWLEDGMENTS

REFERENCES

1. Y.A. Wang and E.A. Carter: Orbital-free kinetic-energy density functional theory. In *Theoretical Methods in Condensed Phase Chemistry*, S.D. Schwartz, ed. (Springer, Dordrecht, 2002); pp. 117–184.
2. H. Chen and A. Zhou: Orbital-free density functional theory for molecular structure calculations. *Numer. Math. Theor. Meth. Appl.* **1**, 1 (2008).
3. T.A. Wesolowski and Y.A. Wang: *Recent Progress in Orbital-Free Density Functional Theory* (World Scientific, Singapore, 2013).
4. V.V. Karasiev, D. Chakraborty, and S.B. Trickey: Progress on new approaches to old ideas: Orbital-free density functionals. In *Many-Electron Approaches in Physics, Chemistry and Mathematics*, V. Bach and L. Delle Site, eds. (Springer, Cham, Switzerland, 2014); pp. 113–134.
5. R.G. Parr and W. Yang: *Density-Functional Theory of Atoms and Molecules* (Oxford University Press, New York, 1994).
6. R.M. Dreizler and E.K.U. Gross: *Density Functional Theory: An Approach to the Quantum Many-Body Problem* (Springer Science & Business Media, 1990).
7. P. Hohenberg and W. Kohn: Inhomogeneous electron gas. *Phys. Rev.* **136**, B864 (1964).
8. W. Kohn and L.J. Sham: Self-consistent equations including exchange and correlation effects. *Phys. Rev.* **140**, A1133 (1965).
9. F. Graziani, M.P. Desjarlais, R. Redmer, and S.B. Trickey: *Frontiers and Challenges in Warm Dense Matter* (Springer Science & Business, Charm, Switzerland, 2014).
10. C.R. Jacob and J. Neugebauer: Subsystem density-functional theory. *Wiley Interdiscip. Rev.: Comput. Mol. Sci.* **4**, 325 (2014).
11. A. Krishtal, D. Sinha, A. Genova, and M. Pavanello: Subsystem density-functional theory as an effective tool for modeling ground and excited states, their dynamics and many-body interactions. *J. Phys.: Condens. Matter* **27**, 183202 (2015).
12. D.R. Bowler and T. Miyazaki: O(N) methods in electronic structure calculations. *Rep. Prog. Phys.* **75**, 036503 (2012).
13. S. Goedecker: Linear scaling electronic structure methods. *Rev. Mod. Phys.* **71**, 1085 (1999).
14. J. Aarons, M. Sarwar, D. Thompsett, and C.-K. Skylaris: Methods for large-scale density functional calculations on metallic systems. *J. Chem. Phys.* **145**, 220901 (2016).
15. E.V. Ludena and V.V. Karasiev: Kinetic energy functionals: History, challenges and prospects. *Rev. Mod. Quantum Chem.* **1**, 612–665 (2002).
16. D. García-Aldea and J.E. Alvarellos: The construction of kinetic energy functionals and the linear response function. In *Theoretical and Computational Developments in Modern Density Functional Theory*, A.K. Roy, ed. (Nova Science Publishers, Hauppauge, New York, 2012), pp. 255–280.
17. C.F. von Weizsäcker: Zur Theorie der Kernmassen. *Z. Phys.* **96**, 431 (1935).
18. L.H. Thomas: The calculation of atomic fields. *Math. Proc. Cambridge Philos. Soc.* **23**, 542 (1927).
19. E. Fermi: Un metodo statistico per la determinazione di alcune priorieta dell'atome. *Rend. Accad. Naz. Lincei* **6**, 32 (1927).
20. J. Lindhard: On the properties of a gas of charged particles. *Kgl. Dan. Vidensk. Selsk.: Mat.-Fys. Medd.* **28**, 8 (1954).
21. F. Perrot: Hydrogen-hydrogen interaction in an electron gas. *J. Phys.: Condens. Matter* **6**, 431 (1994).
22. L.-W. Wang and M.P. Teter: Kinetic-energy functional of the electron density. *Phys. Rev. B* **45**, 13196 (1992).
23. E. Chacón, J.E. Alvarellos, and P. Tarazona: Nonlocal kinetic energy functional for nonhomogeneous electron systems. *Phys. Rev. B* **32**, 7868 (1985).
24. P. García-González, J.E. Alvarellos, and E. Chacón: Nonlocal kinetic-energy-density functionals. *Phys. Rev. B* **53**, 9509 (1996).
25. P. García-González, J.E. Alvarellos, and E. Chacón: Kinetic-energy density functional: Atoms and shell structure. *Phys. Rev. A* **54**, 1897 (1996).
26. P. García-González, J.E. Alvarellos, and E. Chacón: Nonlocal symmetrized kinetic-energy density functional: Application to simple surfaces. *Phys. Rev. B* **57**, 4857 (1998).
27. D. García-Aldea and J.E. Alvarellos: Kinetic-energy density functionals with nonlocal terms with the structure of the Thomas–Fermi functional. *Phys. Rev. A* **76**, 052504 (2007).
28. S. Gómez, L.E. González, D.J. González, M.J. Stott, S. Dalgiç, and M. Silbert: Orbital free ab initio molecular dynamics study of expanded liquid Cs. *J. Non-Cryst. Solids* **250**, 163 (1999).
29. D.J. González, L.E. González, J.M. López, and M.J. Stott: Dynamical properties of liquid Al near melting: An orbital-free molecular dynamics study. *Phys. Rev. B* **65**, 184201 (2002).
30. E. Smargiassi and P.A. Madden: Orbital-free kinetic-energy functionals for first-principles molecular dynamics. *Phys. Rev. B* **49**, 5220 (1994).
31. Y.A. Wang, N. Govind, and E.A. Carter: Orbital-free kinetic-energy functionals for the nearly free electron gas. *Phys. Rev. B* **58**, 13465 (1998).
32. E.H. Lieb: Some open problems about coulomb systems. In *Mathematical Problem in Theoretical Physics*, K. Osterwalder, ed. (Springer, Berlin, Germany, 1979); pp. 91–102.
33. X. Blanc and E. Cancès: Nonlinear instability of density-independent orbital-free kinetic-energy functionals. *J. Chem. Phys.* **122**, 214106 (2005).
34. M. Foley and P.A. Madden: Further orbital-free kinetic-energy functionals for ab initio molecular dynamics. *Phys. Rev. B* **53**, 10589 (1996).
35. Y.A. Wang, N. Govind, and E.A. Carter: Orbital-free kinetic-energy density functionals with a density-dependent kernel. *Phys. Rev. B* **60**, 16350 (1999).
36. G.S. Ho, V.L. Lignères, and E.A. Carter: Analytic form for a nonlocal kinetic energy functional with a density-dependent kernel for orbital-free density functional theory under periodic and Dirichlet boundary conditions. *Phys. Rev. B* **78**, 045105 (2008).
37. B. Zhou, V.L. Lignères, and E.A. Carter: Improving the orbital-free density functional theory description of covalent materials. *J. Chem. Phys.* **122**, 044103 (2005).
38. J.-D. Chai and J.D. Weeks: Modified statistical treatment of kinetic energy in the Thomas–Fermi model. *J. Phys. Chem. B* **108**, 6870 (2004).
39. J.-D. Chai and J.D. Weeks: Orbital-free density functional theory: Kinetic potentials and ab initio local pseudopotentials. *Phys. Rev. B* **75**, 205122 (2007).
40. J.-D. Chai, V.L. Lignères, G. Ho, E.A. Carter, and J.D. Weeks: Orbital-free density functional theory: Linear scaling methods for

kinetic potentials, and applications to solid Al and Si. *Chem. Phys. Lett.* **473**, 263 (2009).

41. C. Huang and E.A. Carter: Nonlocal orbital-free kinetic energy density functional for semiconductors. *Phys. Rev. B* **81**, 045206 (2010).

42. J. Xia, C. Huang, I. Shin, and E.A. Carter: Can orbital-free density functional theory simulate molecules? *J. Chem. Phys.* **136**, 084102 (2012).

43. T.A. Wesolowski and A. Warshel: Frozen density functional approach for ab initio calculations of solvated molecules. *J. Phys. Chem.* **97**, 8050 (1993).

44. G. Senatore and K.R. Subbaswamy: Density dependence of the dielectric constant of rare-gas crystals. *Phys. Rev. B* **34**, 5754 (1986).

45. P. Cortona: Self-consistently determined properties of solids without band-structure calculations. *Phys. Rev. B* **44**, 8454 (1991).

46. N. Govind, Y.A. Wang, and E.A. Carter: Electronic-structure calculations by first-principles density-based embedding of explicitly correlated systems. *J. Chem. Phys.* **110**, 7677 (1999).

47. C. Huang and E.A. Carter: Toward an orbital-free density functional theory of transition metals based on an electron density decomposition. *Phys. Rev. B* **85**, 045126 (2012).

48. J. Xia and E.A. Carter: Density-decomposed orbital-free density functional theory for covalently bonded molecules and materials. *Phys. Rev. B* **86**, 235109 (2012).

49. J. Xia and E.A. Carter: Orbital-free density functional theory study of amorphous Li–Si alloys and introduction of a simple density decomposition formalism. *Modell. Simul. Mater. Sci. Eng.* **24**, 035014 (2016).

50. I. Shin and E.A. Carter: Enhanced von Weizsäcker Wang–Govind–Carter kinetic energy density functional for semiconductors. *J. Chem. Phys.* **140**, 18A531 (2014).

51. P.E. Blöchl: Projector augmented-wave method. *Phys. Rev. B* **50**, 17953 (1994).

52. M. Pearson, E. Smargiassi, and P.A. Madden: Ab initio molecular dynamics with an orbital-free density functional. *J. Phys.: Condens. Matter* **5**, 3221 (1993).

53. I. Shin and E.A. Carter: First-principles simulations of plasticity in body-centered-cubic magnesium–lithium alloys. *Acta Mater.* **64**, 198 (2014).

54. F. Legrain and S. Manzhos: Highly accurate local pseudopotentials of Li, Na, and Mg for orbital free density functional theory. *Chem. Phys. Lett.* **622**(Suppl. C), 99 (2015).

55. B. Wang and M.J. Stott: First-principles local pseudopotentials for group-IV elements. *Phys. Rev. B* **68**, 195102 (2003).

56. B. Zhou, Y.A. Alexander Wang, and E.A. Carter: Transferable local pseudopotentials derived via inversion of the Kohn–Sham equations in a bulk environment. *Phys. Rev. B* **69**, 125109 (2004).

57. S. Watson, B.J. Jesson, E.A. Carter, and P.A. Madden: Ab initio pseudopotentials for orbital-free density functionals. *Europhys. Lett.* **41**, 37 (1998).

58. B. Zhou and E.A. Carter: First principles local pseudopotential for silver: Towards orbital-free density-functional theory for transition metals. *J. Chem. Phys.* **122**, 184108 (2005).

59. C. Huang and E.A. Carter: Transferable local pseudopotentials for magnesium, aluminum and silicon. *Phys. Chem. Chem. Phys.* **10**, 7109 (2008).

60. M. Chen, L. Hung, C. Huang, J. Xia, and E.A. Carter: The melting point of lithium: An orbital-free first-principles molecular dynamics study. *Mol. Phys.* **111**, 3448 (2013).

61. M. Chen, J.R. Vella, A.Z. Panagiotopoulos, P.G. Debenedetti, F.H. Stillinger, and E.A. Carter: Liquid Li structure and dynamics: A comparison between OFDFT and second nearest-neighbor embedded-atom method. *AIChE J.* **61**, 2841 (2015).

62. J.M. Ziman: The method of neutral pseudo-atoms in the theory of metals. *Adv. Phys.* **13**, 89 (1964).

63. L. Dagens: A selfconsistent calculation of the rigid neutral atom density according to the auxiliary neutral atom model. *J. Phys. C: Solid State Phys.* **5**, 2333 (1972).

64. J.A. Anta and P.A. Madden: Structure and dynamics of liquid lithium: Comparison of ab initio molecular dynamics predictions with scattering experiments. *J. Phys.: Condens. Matter* **11**, 6099 (1999).

65. L.E. González, D.J. González, and J.M. López: Pseudopotentials for the calculation of dynamic properties of liquids. *J. Phys.: Condens. Matter* **13**, 7801 (2001).

66. B.G. del Rio and L.E. González: Orbital free ab initio simulations of liquid alkaline earth metals: From pseudopotential construction to structural and dynamic properties. *J. Phys.: Condens. Matter* **26**, 465102 (2014).

67. B.G. del Rio, J.M. Dieterich, and E.A. Carter: Globally-optimized local pseudopotentials for (orbital-free) density functional theory simulations of liquids and solids. *J. Chem. Theory Comput.* **13**, 3684 (2017).

68. S.C. Watson and E.A. Carter: Linear-scaling parallel algorithms for the first principles treatment of metals. *Comput. Phys. Commun.* **128**, 67 (2000).

69. G.S. Ho, V.L. Lignères, and E.A. Carter: Introducing PROFESS: A new program for orbital-free density functional theory calculations. *Comput. Phys. Commun.* **179**, 839 (2008).

70. L. Hung, C. Huang, I. Shin, G.S. Ho, V.L. Lignères, and E.A. Carter: Introducing PROFESS 2.0: A parallelized, fully linear scaling program for orbital-free density functional theory calculations. *Comput. Phys. Commun.* **181**, 2208 (2010).

71. M. Chen, J. Xia, C. Huang, J.M. Dieterich, L. Hung, I. Shin, and E.A. Carter: Introducing PROFESS 3.0: An advanced program for orbital-free density functional theory molecular dynamics simulations. *Comput. Phys. Commun.* **190**, 228 (2015).

72. V.V. Karasiev, T. Sjostrom, and S.B. Trickey: Finite-temperature orbital-free DFT molecular dynamics: Coupling PROFESS and Quantum Espresso. *Comput. Phys. Commun.* **185**, 3240 (2014).

73. S. Das, M. Iyer, and V. Gavini: Real-space formulation of orbital-free density functional theory using finite-element discretization: The case for Al, Mg, and Al–Mg intermetallics. *Phys. Rev. B* **92**, 014104 (2015).

74. J. Lehtomäki, I. Makkonen, M.A. Caro, A. Harju, and O. Lopez-Acevedo: Orbital-free density functional theory implementation with the projector augmented-wave method. *J. Chem. Phys.* **141**, 234102 (2014).

75. W. Mi, X. Shao, C. Su, Y. Zhou, S. Zhang, Q. Li, H. Wang, L. Zhang, M. Miao, Y. Wang, and Y. Ma: ATLAS: A real-space finite-difference implementation of orbital-free density functional theory. *Comput. Phys. Commun.* **200**, 87 (2016).

76. V.L. Lignères and E.A. Carter: An introduction to orbital-free density functional theory. In *Handbook of Materials Modeling*, S. Yip, ed. (Springer, Dordrecht, 2005); pp. 137–148.

77. L. Hung and E.A. Carter: Accurate simulations of metals at the mesoscale: Explicit treatment of 1 million atoms with quantum mechanics. *Chem. Phys. Lett.* **475**, 163 (2009).

78. U. Essmann, L. Perera, M.L. Berkowitz, T. Darden, H. Lee, and L.G. Pedersen: A smooth particle mesh Ewald method. *J. Chem. Phys.* **103**, 8577 (1995).

79. N. Choly and E. Kaxiras: Fast method for force computations in electronic structure calculations. *Phys. Rev. B* **67**, 155101 (2003).

80. A. Gupta and V. Kumar: The scalability of FFT on parallel computers. *IEEE Trans. Parallel Distrib. Syst.* **4**, 922 (1993).

81. M. Chen, X.-W. Jiang, H. Zhuang, L.-W. Wang, and E.A. Carter: Petascale orbital-free density functional theory enabled by small-box algorithms. *J. Chem. Theory Comput.* **12**, 2950 (2016).

82. J.M. Dieterich, W.C. Witt, and E.A. Carter: libKEDF: An accelerated library of kinetic energy density functionals. *J. Comput. Chem.* **38**, 1552 (2017).

83. V. Gavini, J. Knap, K. Bhattacharya, and M. Ortiz: Non-periodic finite-element formulation of orbital-free density functional theory. *J. Mech. Phys. Solids* **55**, 669 (2007).

84. B. Radhakrishnan and V. Gavini: Orbital-free density functional theory study of the energetics of vacancy clustering and prismatic dislocation loop nucleation in aluminium. *Philos. Mag.* **96**, 2468 (2016).

85. P. Motamarri, M. Iyer, J. Knap, and V. Gavini: Higher-order adaptive finite-element methods for orbital-free density functional theory. *J. Comput. Phys.* **231**, 6596 (2012).

86. N. Choly and E. Kaxiras: Kinetic energy density functionals for non-periodic systems. *Solid State Commun.* **121**, 281 (2002).

87. V. Gavini, K. Bhattacharya, and M. Ortiz: Quasi-continuum orbital-free density-functional theory: A route to multi-million atom non-periodic DFT calculation. *J. Mech. Phys. Solids* **55**, 697 (2007).

88. L. Hung, C. Huang, and E.A. Carter: Preconditioners and electron density optimization in orbital-free density functional theory. *Commun. Comput. Phys.* **12**, 135 (2012).

89. M. Fago, R.L. Hayes, E.A. Carter, and M. Ortiz: Density-functional-theory-based local quasicontinuum method: Prediction of dislocation nucleation. *Phys. Rev. B* **70**, 100102 (2004).

90. N. Choly, G. Lu, W. E, and E. Kaxiras: Multiscale simulations in simple metals: A density-functional-based methodology. *Phys. Rev. B* **71**, 094101 (2005).

91. B.G. Radhakrishnan and V. Gavini: Electronic structure calculations at macroscopic scales using orbital-free DFT. In *Recent Progress in Orbital-Free Density Functional Theory*, T.A. Wesolowski and Y.A. Wang, eds. (World Scientific, Singapore, 2013), pp. 147–163.

92. R.O. Jones and O. Gunnarsson: The density functional formalism, its applications and prospects. *Rev. Mod. Phys.* **61**, 689 (1989).

93. D.B. Miracle and O.N. Senkov: A critical review of high entropy alloys and related concepts. *Acta Mater.* **122**, 448 (2017).

94. K.M. Carling and E.A. Carter: Orbital-free density functional theory calculations of the properties of Al, Mg and Al–Mg crystalline phases. *Modell. Simul. Mater. Sci. Eng.* **11**, 339 (2003).

95. H. Zhuang, M. Chen, and E.A. Carter: Elastic and thermodynamic properties of complex Mg–Al intermetallic compounds via orbital-free density functional theory. *Phys. Rev. Appl.* **5**, 064021 (2016).

96. H.L. Zhuang, M. Chen, and E.A. Carter: Prediction and characterization of an Mg–Al intermetallic compound with potentially improved ductility via orbital-free and Kohn–Sham density functional theory. *Modell. Simul. Mater. Sci. Eng.* **25**, 075002 (2017).

97. J. Xia and E.A. Carter: Orbital-free density functional theory study of crystalline Li–Si alloys. *J. Power Sources* **254**, 62 (2014).

98. G. Ho, M.T. Ong, K.J. Caspersen, and E.A. Carter: Energetics and kinetics of vacancy diffusion and aggregation in shocked aluminium via orbital-free density functional theory. *Phys. Chem. Chem. Phys.* **9**, 4951 (2007).

99. B. Radhakrishnan and V. Gavini: Effect of cell size on the energetics of vacancies in aluminum studied via orbital-free density functional theory. *Phys. Rev. B* **82**, 094117 (2010).

100. R. Qiu, H. Lu, B. Ao, L. Huang, T. Tang, and P. Chen: Energetics of intrinsic point defects in aluminium via orbital-free density functional theory. *Philos. Mag.* **97**, 2164 (2017).

101. R. Hayes, M. Fago, M. Ortiz, and E. Carter: Prediction of dislocation nucleation during nanoindentation by the orbital-free density functional theory local quasi-continuum method. *Multiscale Model. Simul.* **4**, 359 (2005).

102. R.L. Hayes, G. Ho, M. Ortiz, and E.A. Carter: Prediction of dislocation nucleation during nanoindentation of Al_3Mg by the orbital-free density functional theory local quasicontinuum method. *Philos. Mag.* **86**, 2343 (2006).

103. Q. Peng, X. Zhang, C. Huang, E.A. Carter, and G. Lu: Quantum mechanical study of solid solution effects on dislocation nucleation during nanoindentation. *Modell. Simul. Mater. Sci. Eng.* **18**, 075003 (2010).

104. E.B. Tadmor, M. Ortiz, and R. Phillips: Quasicontinuum analysis of defects in solids. *Philos. Mag. A* **73**, 1529 (1996).

105. E.B. Tadmor, R. Phillips, and M. Ortiz: Mixed atomistic and continuum models of deformation in solids. *Langmuir* **12**, 4529 (1996).

106. Q. Peng, X. Zhang, L. Hung, E.A. Carter, and G. Lu: Quantum simulation of materials at micron scales and beyond. *Phys. Rev. B* **78**, 054118 (2008).

107. G.S. Ho, C. Huang, and E.A. Carter: Describing metal surfaces and nanostructures with orbital-free density functional theory. *Curr. Opin. Solid State Mater. Sci.* **11**, 57 (2007).

108. X. Zhang and G. Lu: Calculation of fast pipe diffusion along a dislocation stacking fault ribbon. *Phys. Rev. B* **82**, 012101 (2010).

109. I. Shin, A. Ramasubramaniam, C. Huang, L. Hung, and E.A. Carter: Orbital-free density functional theory simulations of dislocations in aluminum. *Philos. Mag.* **89**, 3195 (2009).

110. M. Iyer, B. Radhakrishnan, and V. Gavini: Electronic-structure study of an edge dislocation in aluminum and the role of macroscopic deformations on its energetics. *J. Mech. Phys. Solids* **76**, 260 (2015).

111. S. Das and V. Gavini: Electronic structure study of screw dislocation core energetics in aluminum and core energetics informed forces in a dislocation aggregate. *J. Mech. Phys. Solids* **104**, 115 (2017).

112. I. Shin and E.A. Carter: Orbital-free density functional theory simulations of dislocations in magnesium. *Modell. Simul. Mater. Sci. Eng.* **20**, 015006 (2012).

113. I. Shin and E.A. Carter: Possible origin of the discrepancy in Peierls stresses of fcc metals: First-principles simulations of dislocation mobility in aluminum. *Phys. Rev. B* **88**, 064106 (2013).

114. I. Shin and E.A. Carter: Simulations of dislocation mobility in magnesium from first principles. *Int. J. Plast.* **60**, 58 (2014).

115. S.C. Watson and P.A. Madden: Grain boundary migration at finite temperature: An ab initio molecular dynamics study. *PhysChemComm* **1**, 1 (1998).

116. L. Hung and E.A. Carter: Ductile processes at aluminium crack tips: Comparison of orbital-free density functional theory with classical potential predictions. *Modell. Simul. Mater. Sci. Eng.* **19**, 045002 (2011).

117. A. Aguado, D.J. González, L.E. González, J.M. López, S. Núñez, and M.J. Stott: An orbital free ab initio method: Applications to liquid metals and clusters. In *Recent Progress in Orbital-Free Density Functional Theory*, T.A. Wesolowski and Y.A. Yang, eds. (World Scientific Publishing Company, Singapore, 2013), pp. 55–145.

118. G.S. Ho and E.A. Carter: Mechanical response of aluminum nanowires via orbital-free density functional theory. *J. Comput. Theor. Nanosci.* **6**, 1236 (2009).

119. L. Hung and E.A. Carter: Orbital-free DFT simulations of elastic response and tensile yielding of ultrathin [111] Al nanowires. *J. Phys. Chem. C* **115**, 6269 (2011).

120. M. Foley, E. Smargiassi, and P.A. Madden: The dynamic structure of liquid sodium from ab initio simulation. *J. Phys.: Condens. Matter* **6**, 5231 (1994).

121. J.A. Anta, B.J. Jesson, and P.A. Madden: Ion-electron correlations in liquid metals from orbital-free ab initio molecular dynamics. *Phys. Rev. B* **58**, 6124 (1998).

122. S. Şengül, D.J. González, and L.E. González: Structural and dynamical properties of liquid Mg. An orbital-free molecular dynamics study. *J. Phys.: Condens. Matter* **21**, 115106 (2009).

123. D.J. González, L.E. González, J.M. López, and M.J. Stott: Orbital free ab initio molecular dynamics study of liquid Al near melting. *J. Chem. Phys.* **115**, 2373 (2001).

124. T.G. White, S. Richardson, B.J.B. Crowley, L.K. Pattison, J.W.O. Harris, and G. Gregori: Orbital-free density-functional theory simulations of the dynamic structure factor of warm dense aluminum. *Phys. Rev. Lett.* **111**, 175002 (2013).

125. T. Sjostrom and J. Daligault: Ionic and electronic transport properties in dense plasmas by orbital-free density functional theory. *Phys. Rev. E* **92**, 063304 (2015).

126. L.E. González and D.J. González: Structure and dynamics of bulk liquid Ga and the liquid–vapor interface: An ab initio study. *Phys. Rev. B* **77**, 064202 (2008).

127. A. Delisle, D.J. González, and M.J. Stott: Structural and dynamical properties of liquid Si: An orbital-free molecular dynamics study. *Phys. Rev. B* **73**, 064202 (2006).

128. A. Delisle, D.J. González, and M.J. Stott: Pressure-induced structural and dynamical changes in liquid Si—An ab initio study. *J. Phys.: Condens. Matter* **18**, 3591 (2006).

129. G. Jacucci, M. Ronchetti, and W. Schirmacher: Computer simulation of the liquid Li₄Pb alloy. *J. Phys., Colloq.* **46**, C8 (1985).

130. A. Campa and E.G.D. Cohen: Fast sound in binary fluid mixtures. *Phys. Rev. A* **41**, 5451 (1990).

131. P. Westerhuijs, W. Montfrooij, L.A. de Graaf, and I.M. de Schepper: Fast and slow sound in a dense gas mixture of helium and neon. *Phys. Rev. A* **45**, 3749 (1992).

132. J. Blanco, D.J. González, L.E. González, J.M. López, and M.J. Stott: Collective ionic dynamics in the liquid Na–Cs alloy: An ab initio molecular dynamics study. *Phys. Rev. E* **67**, 041204 (2003).

133. D.J. González, L.E. González, J.M. López, and M.J. Stott: Microscopic dynamics in the liquid Li–Na alloy: An ab initio molecular dynamics study. *Phys. Rev. E* **69**, 031205 (2004).

134. J.S. Rowlinson and B. Widom: *Molecular Theory of Capillarity* (Clarendon Press, Oxford, U.K., 1982).

135. B.M. Ocko, X.Z. Wu, E.B. Sirota, S.K. Sinha, and M. Deutsch: X-ray reflectivity study of thermal capillary waves on liquid surfaces. *Phys. Rev. Lett.* **72**, 242 (1994).

136. M.J. Regan, E.H. Kawamoto, S. Lee, P.S. Pershan, N. Maskil, M. Deutsch, O.M. Magnussen, B.M. Ocko, and L.E. Berman: Surface layering in liquid gallium: An X-ray reflectivity study. *Phys. Rev. Lett.* **75**, 2498 (1995).

137. M.J. Regan, P.S. Pershan, O.M. Magnussen, B.M. Ocko, M. Deutsch, and L.E. Berman: X-ray reflectivity studies of liquid metal and alloy surfaces. *Phys. Rev. B* **55**, 15874 (1997).

138. G. Fabricius, E. Artacho, D. Sánchez-Portal, P. Ordejón, D.A. Drabold, and J.M. Soler: Atomic layering at the liquid silicon surface: A first-principles simulation. *Phys. Rev. B* **60**, R16283 (1999).

139. B.G. Walker, N. Marzari, and C. Molteni: Ab initio studies of layering behavior of liquid sodium surfaces and interfaces. *J. Chem. Phys.* **124**, 174702 (2006).

140. D.J. González, L.E. González, and M.J. Stott: Surface structure of liquid Li and Na: An ab initio molecular dynamics study. *Phys. Rev. Lett.* **92**, 085501 (2004).

141. D.J. González, L.E. González, and M.J. Stott: Surface structure in simple liquid metals: An orbital-free first-principles study. *Phys. Rev. B* **74**, 014207 (2006).

142. D.J. González and L.E. González: Structure of the liquid–vapor interfaces of Ga, in and the eutectic Ga–In alloy—an ab initio study. *J. Phys.: Condens. Matter* **20**, 114118 (2008).

143. D.J. González, L.E. González, and M.J. Stott: Liquid-vapor interface in liquid binary alloys: An ab initio molecular dynamics study. *Phys. Rev. Lett.* **94**, 077801 (2005).

144. D.J. González and L.E. González: Structure and motion at the liquid-vapor interface of some interalkali binary alloys: An orbital-free ab initio study. *J. Chem. Phys.* **130**, 114703 (2009).

145. B.J. Jesson and P.A. Madden: Structure and dynamics at the aluminum solid–liquid interface: An ab initio simulation. *J. Chem. Phys.* **113**, 5935 (2000).

146. L.E. González and D.J. González: Orbital-free ab-initio study of the structure of liquid Al on a model fcc metallic wall: The influence of surface orientation. *J. Phys.: Conf. Ser.* **98**, 062024 (2008).

147. D.K. Chokappa and P. Clancy: A computer simulation study of the melting and freezing properties of a system of Lennard-Jones particles. *Mol. Phys.* **61**, 597 (1987).

148. J.R. Morris, C.Z. Wang, K.M. Ho, and C.T. Chan: Melting line of aluminum from simulations of coexisting phases. *Phys. Rev. B* **49**, 3109 (1994).

149. A.B. Belonoshko, N.V. Skorodumova, A. Rosengren, and B. Johansson: Melting and critical superheating. *Phys. Rev. B* **73**, 012201 (2006).

150. E. Gregoryanz, L.F. Lundegaard, M.I. McMahon, C. Guillaume, R.J. Nelmes, and M. Mezouar: Structural diversity of sodium. *Science* **320**, 1054 (2008).

151. M. Marqués, M.I. McMahon, E. Gregoryanz, M. Hanfland, C.L. Guillaume, C.J. Pickard, G.J. Ackland, and R.J. Nelmes: Crystal structures of dense lithium: A metal-semiconductor-metal transition. *Phys. Rev. Lett.* **106**, 095502 (2011).

152. M. Marqués, D.J. González, and L.E. González: Structure and dynamics of high-pressure Na close to the melting line: An ab initio molecular dynamics study. *Phys. Rev. B* **94**, 024204 (2016).

153. J.P. Perdew and L.A. Constantin: Laplacian-level density functionals for the kinetic energy density and exchange-correlation energy. *Phys. Rev. B* **75**, 155109 (2007).

154. S. Śmiga, E. Fabiano, L.A. Constantin, and F. Della Sala: Laplacian-dependent models of the kinetic energy density: Applications in subsystem density functional theory with meta-generalized gradient approximation functionals. *J. Chem. Phys.* **146**, 064105 (2017).

155. F. Tran and T.A. Wesolowski: Semilocal approximations for the kinetic energy. In *Recent Progress in Orbital-Free Density Functional Theory*, T.A. Wesolowski and Y.A. Wang, eds. (World Scientific, Singapore, 2012); pp. 429–442.

156. V.V. Karasiev, R.S. Jones, S.B. Trickey, and F.E. Harris: Properties of constraint-based single-point approximate kinetic energy functionals. *Phys. Rev. B* **80**, 245120 (2009).

157. V.V. Karasiev, D. Chakraborty, O.A. Shukruto, and S.B. Trickey: Nonempirical generalized gradient approximation free-energy functional for orbital-free simulations. *Phys. Rev. B* **88**, 161108 (2013).

158. V.V. Karasiev and S.B. Trickey: Frank discussion of the status of ground-state orbital-free DFT. In *Advances in Quantum Chemistry*, J.R. Sabin and R. Cabrera-Trujillo, eds. (Academic Press, London, U.K., 2015); pp. 221–245.

159. A.C. Cancio, D. Stewart, and A. Kuna: Visualization and analysis of the Kohn–Sham kinetic energy density and its orbital-free description in molecules. *J. Chem. Phys.* **144**, 084107 (2016).

794

J. Mater. Res., Vol. 33, No. 7, Apr 13, 2018

160. J. Xia and E.A. Carter: Single-point kinetic energy density functionals: A pointwise kinetic energy density analysis and numerical convergence investigation. *Phys. Rev. B* **91**, 045124 (2015).

161. S.B. Trickey, V.V. Karasiev, and D. Chakraborty: Comment on "Single-point kinetic energy density functionals: A pointwise kinetic energy density analysis and numerical convergence investigation". *Phys. Rev. B* **92**, 117101 (2015).

162. J. Xia and E.A. Carter: Reply to "comment on 'Single-point kinetic energy density functionals: A pointwise kinetic energy density analysis and numerical convergence investigation'". *Phys. Rev. B* **92**, 117102 (2015).

163. F. Della Sala, E. Fabiano, and L.A. Constantin: Kohn–Sham kinetic energy density in the nuclear and asymptotic regions: Deviations from the von Weizsäcker behavior and applications to density functionals. *Phys. Rev. B* **91**, 035126 (2015).

164. K. Finzel: Local conditions for the Pauli potential in order to yield self-consistent electron densities exhibiting proper atomic shell structure. *J. Chem. Phys.* **144**, 034108 (2016).

165. P. Elliott, D. Lee, A. Cangi, and K. Burke: Semiclassical origins of density functionals. *Phys. Rev. Lett.* **100**, 256406 (2008).

166. D. Lee, L.A. Constantin, J.P. Perdew, and K. Burke: Condition on the Kohn–Sham kinetic energy and modern parametrization of the Thomas–Fermi density. *J. Chem. Phys.* **130**, 034107 (2009).

167. L.A. Constantin, E. Fabiano, S. Laricchia, and F. Della Sala: Semiclassical neutral atom as a reference system in density functional theory. *Phys. Rev. Lett.* **106**, 186406 (2011).

168. E. Fabiano and L.A. Constantin: Relevance of coordinate and particle-number scaling in density-functional theory. *Phys. Rev. A* **87**, 012511 (2013).

169. A.C. Cancio and J.J. Redd: Visualisation and orbital-free parametrisation of the large-Z scaling of the kinetic energy density of atoms. *Mol. Phys.* **115**, 618 (2017).

170. K. Finzel: Shell-structure-based functionals for the kinetic energy. *Theor. Chem. Acc.* **134**, 106 (2015).

171. L.A. Constantin and A. Ruzsinszky: Kinetic energy density functionals from the Airy gas with an application to the atomization kinetic energies of molecules. *Phys. Rev. B* **79**, 115117 (2009).

172. A. Lindmaa, A.E. Mattsson, and R. Armiento: Quantum oscillations in the kinetic energy density: Gradient corrections from the Airy gas. *Phys. Rev. B* **90**, 075139 (2014).

173. L.A. Constantin, E. Fabiano, S. Śmiga, and F. Della Sala: Jellium-with-gap model applied to semilocal kinetic functionals. *Phys. Rev. B* **95**, 115153 (2017).

174. L.A. Constantin, E. Fabiano, and F. Della Sala: Modified fourth-order kinetic energy gradient expansion with hartree potential-dependent coefficients. *J. Chem. Theory Comput.* **13**, 4228 (2017).

175. Y. Ke, F. Libisch, J. Xia, L-W. Wang, and E.A. Carter: Angular-momentum-dependent orbital-free density functional theory. *Phys. Rev. Lett.* **111**, 066402 (2013).

176. Y. Ke, F. Libisch, J. Xia, and E.A. Carter: Angular momentum dependent orbital-free density functional theory: Formulation and implementation. *Phys. Rev. B* **89**, 155112 (2014).